

Time-Resolved and Mechanistic Study of the Photochemical Uncaging Reaction of the *o*-Hydroxycinnamic Caged Compound

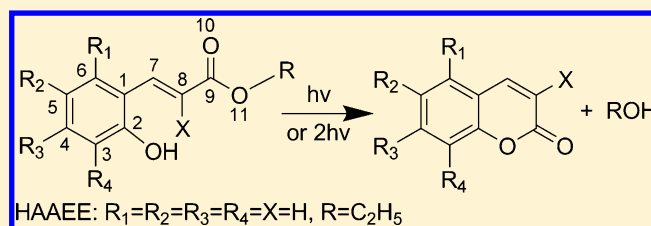
Youqing Yu, Lidan Wu, Xiaoran Zou, Xiaojuan Dai, Kunhui Liu, and Hongmei Su*

Beijing National Laboratory for Molecular Sciences (BNLMS), State Key Laboratory of Molecular Reaction Dynamics, Institute of Chemistry, Chinese Academy of Sciences, Beijing 100190, China

Supporting Information

ABSTRACT: The *o*-hydroxycinnamic derivatives represent efficient caged compounds that can realize quantification of delivery upon uncaging, but there has been lack of time-resolved and mechanistic studies. We used time-resolved infrared (TRIR) spectroscopy to investigate the photochemical uncaging dynamics of the prototype *o*-hydroxycinnamic compound, (*E*)-3-(2-hydroxyphenyl)acrylic acid ethyl ester (HAAEE), leading to coumarin and ethanol upon uncaging.

Taking advantage of the specific vibrational marker bands and the IR discerning capability, we have identified and distinguished two key intermediate species, the *cis*-isomers of HAAEE and the tetrahedral intermediate, in the transient infrared spectra, thus providing clear spectral evidence to support the intramolecular nucleophilic addition mechanism following the *trans*–*cis* photoisomerization. Moreover, the product yields of coumarin upon uncaging were observed to be greatly affected by the solvent polarity, suppressed in CH₂Cl₂ but enhanced in D₂O/CH₃CN with the increasing volume ratio of D₂O. The highly solvent-dependent behavior indicates E1 elimination of the tetrahedral intermediate to give rise to the final uncaging product coumarin. The photorelease rate of coumarin was directly characterized from TRIR ($3.6 \times 10^6 \text{ s}^{-1}$), revealing the promising application of such *o*-hydroxycinnamic compound in producing fast alcohol jumps. The TRIR results provide the first time-resolved detection and thus offer direct dynamical information about this photochemical uncaging reaction.



1. INTRODUCTION

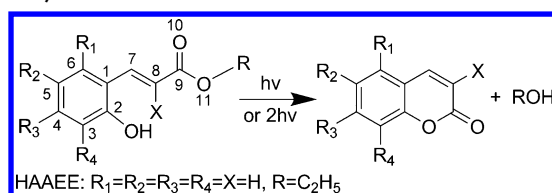
Photolabile protecting groups and caged compounds have been widely used in chemical and biological studies.^{1–4} Their attractiveness comes from the possibility of controlling both the location and the time of release of active chemicals by exposure to light alone. A large variety of such protecting groups have been developed, each of them tailored for specific uses.^{5–8} Among them, developing phototriggers that can realize quantification of delivery upon uncaging is of particular importance when a critical molecule concentration is required to induce a specific activity.

The *o*-hydroxycinnamic group to cage alcohols and amines has received strong interest in this regard.^{9–13} The cinnamate backbones in the caged precursor intrinsically do not fluoresce, while the photoreleased coumarin coproduct is fluorescent (Scheme 1) and can serve as a fluorescent reporter. Quantification of delivery upon uncaging could be then simply

achieved by analyzing the increase of fluorescence emission after or during uncaging at the targeted site. Moreover, the *o*-hydroxycinnamic group has sufficient sensitivity to both one-photon excitation (1PE) and two-photon excitation (2PE),^{11,12} while chromophores that can act as a 2PE photoremovable protecting group for biological use are rare.^{14,15} Attributed to these advantages, *o*-hydroxycinnamic platform is particularly attractive in tailoring photolabile protecting groups that exhibit large two-photon uncaging cross-sections and that release strongly fluorescent coproducts upon uncaging, and thus holds practical potential as an efficient cage for the liberation of various biological stimulants.^{9–13}

For rational design of novel caging groups using *o*-hydroxycinnamic derivatives, it is important to understand the detailed mechanism concerning how the photochemical uncaging reaction occurs. The products and conditions for the *o*-hydroxycinnamic uncaging have been well established in previous work.^{9–13} In addition, an intramolecular nucleophilic addition mechanism was proposed to account for the uncaging process (Scheme 2), which involves the *trans*–*cis* photoisomerization followed by the nucleophilic addition of the *o*-hydroxy group onto the ethyl ester moiety forming the tetrahedral intermediate, prior to releasing ethanol and the

Scheme 1. Photochemical Uncaging Reaction of (*E*)-*o*-Hydroxycinnamates to Coumarin and Alcohol

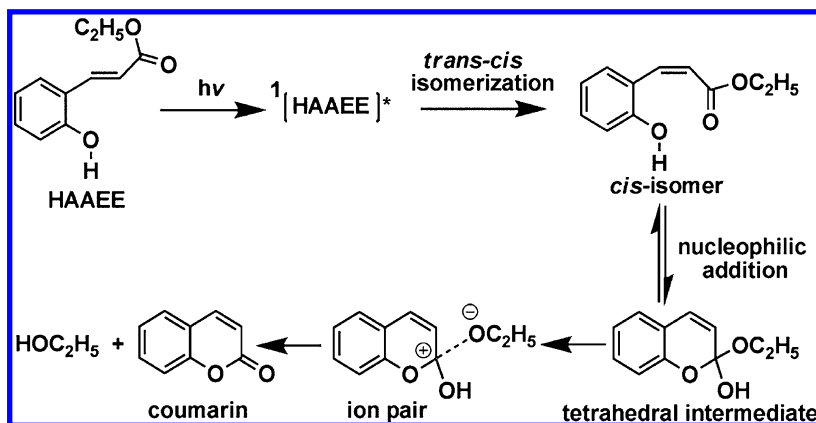


Received: October 11, 2012

Revised: July 12, 2013

Published: July 19, 2013

Scheme 2. Proposed Reaction Mechanism for the Photochemical Uncaging of HAAEE



coumarin coproduct. However, there is some uncertainty of discerning tetrahedral intermediate from the cis-isomers in the ^1H NMR spectra,^{11,16} for both species have an identical C7=C8 double bond with (*Z*) stereochemistry. Unambiguous identification of the reaction intermediates is thus desirable to establish the uncaging mechanism. Meanwhile, the mechanisms concerning the releasing of coumarin from tetrahedral intermediate are required to be explored further.

Another important issue that is critical to the use of the caged compound is the rate of the photolytic release of the substrate from these inert precursors.⁸ Nevertheless, it has been lack of time-resolved measurements of the photorelease rate for the *o*-hydroxycinnamic caged compounds. Transient UV–visible absorption measurements could be a sensitive probe for this rate.^{17–19} However, this method suffers from an inability to distinguish the photoreleased coumarin coproduct from its cinnamate precursor because the two absorb UV–visible light in the same wavelength range.¹¹ Alternatively, the step-scan FTIR spectroscopy in the nanosecond time domain^{8,20} offers a direct, noninferential time-resolved method to determine the rate of release where the photoreleased product exhibits specific vibrational signatures. A time-resolved infrared (TRIR) investigation using the vibrational marker bands would therefore allow for the direct characterization of the photorelease rate of the uncaged products.

In these regards, we report here a TRIR investigation on the photochemical uncaging dynamics of the *o*-hydroxycinnamic caging group represented by the prototype *o*-hydroxycinnamic caged compound, the (*E*)-3-(2-hydroxyphenyl)-acrylic acid ethyl ester (denoted as HAAEE in Scheme 1) leading to the release of coumarin and ethanol upon uncaging. TRIR experiments were performed to directly probe and determine formation dynamics of the uncaged products from photoexcited HAAEE in $\text{D}_2\text{O}/\text{CH}_3\text{CN}$ mixed solvents with varying water concentration as well as in other typical solvents such as CH_2Cl_2 . It is expected that comparison of the real time reaction dynamics in different solvents can provide important evidence to help elucidate the nature of the photorelease mechanism of the *o*-hydroxycinnamic caged compound. In addition, the key transient intermediates can be identified in the TRIR spectra by their characteristic vibrational marker bands, thus providing spectral evidence to establish the reaction mechanism. To the best of our knowledge, the TRIR results presented here provide the first direct time-resolved detection of the photochemical uncaging reaction for *o*-hydroxycinnamic phototrigger compounds.

2. EXPERIMENTAL AND COMPUTATIONAL METHODS

2.1. Experiments. **2.1.1. Materials.** (*E*)-3-(2-Hydroxyphenyl)-acrylic acid ethyl ester (HAAEE) (>96%) and D_2O (>99%) was purchased from Sigma Aldrich and used as received. Solvents of chromatographic grade (CH_3CN and CH_2Cl_2) were used.

2.1.2. Time-Resolved Fourier Transform IR (TR-FTIR) Experiment. Detailed experimental procedures for step-scan, time-resolved Fourier transform IR (TR-FTIR) absorption spectroscopy^{21,22} have been described in our previous publications.²³ Briefly, the TR-FTIR instrument (setup shown in Figure 1) comprises a Nicolet Nexus 870

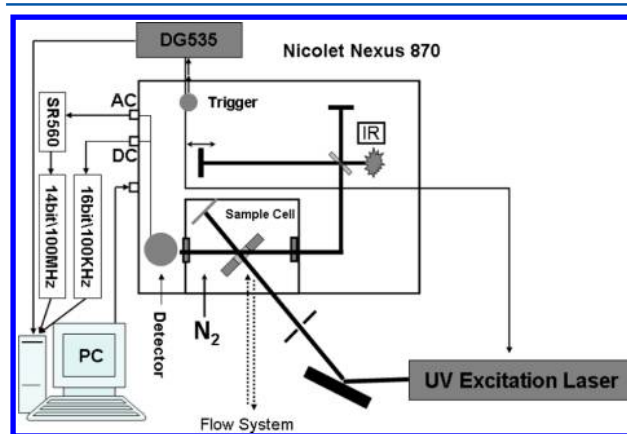


Figure 1. Schematic representation of the TR-FTIR experimental setup.

spectrometer, Continuum Surelite II Nd YAG laser, and a pulse generator (Stanford Research DG535) to initiate the laser pulse and achieve synchronization of the laser with data collection, two digitizers (internal 100kHz 16-bit digitizer and external 100 MHz 14-bit GAGE 14100 digitizer), which offer fast time resolution and a wide dynamic range as needed, and a personal computer to control the whole experiment. The detector used in this work is the photovoltaic MCT (0.5 mm) equipped with a fast internal preamplifier (50 MHz).

There are two outputs from the detector: output DC, corresponding to the value of the static interferogram; and output AC, corresponding to the time-resolved change of the interferogram. The AC signal was then amplified by an external preamplifier (Stanford Research, SRS560). The differential absorbance spectra are calculated based on the equation where

I_{DC} and ΔI_{AC} are the single-beam intensity spectra corresponding to static (DC) and dynamic (AC) channels. ΔI_{AC} is calibrated before being used in equation because different gain is applied to the AC channel.^{21,22}

The fourth harmonic of Nd YAG laser (266 nm) operating at 10 Hz repetition rate was used in the experiments. The laser excitation beam was directed through an iris aperture (3 mm in diameter) and then overlapped with the infrared beam in the sample cell within the sample compartment of the FTIR spectrometer. The laser beam energy after the aperture was 1 mJ per pulse. The IR spectra were collected with a spectral resolution of 8 cm^{-1} . A Harrick flowing solution cell with 2 mm thick CaF_2 windows (path-length, $100\ \mu\text{m}$) was used for the measurements. The closed flowing system is driven by a peristaltic pump (ColeParmer Masterflex) to refresh the sample before every laser pulse.

2.1.3. Steady-State UV–Vis Absorption Experiment. Absorption spectra were recorded with a UV–vis spectrometer (Model U-3010, Hitachi) in a 10 mm path length quartz cuvette.

2.2. Computational Methods. We have calculated the potential energy profile for the possible intramolecular nucleophilic addition mechanism of HAAEE toward releasing ethanol and coumarin. The geometries of the reactants, products, intermediates, and transition states along the reaction route are optimized using the hybrid density functional theory, i.e., Becke's three-parameter nonlocal exchange functional with the nonlocal correlation functional of Lee, Yang, and Parr (B3LYP) with the 6-311++G(d, p) basis sets.^{24,25} Harmonic vibrational frequencies, relative energies, and the zero-point energies (ZPE) are calculated at the same level with the optimized geometries. The intermediates are characterized by all the real frequencies. The transition states are confirmed by only one imaginary frequency. Connections of the transition states between two local minima have been confirmed by intrinsic reaction coordinate (IRC) calculations at the same level.²⁶ Bulk solvation effects are considered using the polarized continuum model (PCM).^{27,28}

Geometry optimizations of ground-state HAAEE, cis-isomers of HAAEE, tetrahedral intermediate, coumarin, and triplet-state HAAEE were performed at the B3LYP/6-311++G(d,p) level of theory. Tight optimization criteria were used in all calculations. All stationary points were confirmed to be energy minima using vibrational frequency calculations (B3LYP/6-311++G(d,p)), which confirmed that all of the computed vibrational frequencies were real (i.e., no imaginary vibrational frequencies). To aid with spectral assignments, vibrational frequencies were calculated in both the vacuum and in solvents under the polarized continuum model. Using the ground-state stationary structures, the vertical electronic excitations were calculated with time-dependent DFT at the TD-B3LYP/6-311++G(d,p) level of theory. Difference density plots were generated from the computed electron densities of the ground and excited states (TD-B3LYP/6-311++G(d,p)). All of the theoretical calculations were performed with the Gaussian03 program package.²⁹

3. RESULTS AND DISCUSSION

Steady-state infrared absorption spectra of HAAEE in CH_3CN were recorded before and after UV irradiation at 266 nm, in order to locate IR marker bands that are indicative of the photoreleased uncaging product. In the spectrum obtained before UV irradiation (red curve in Figure 2a), three strong

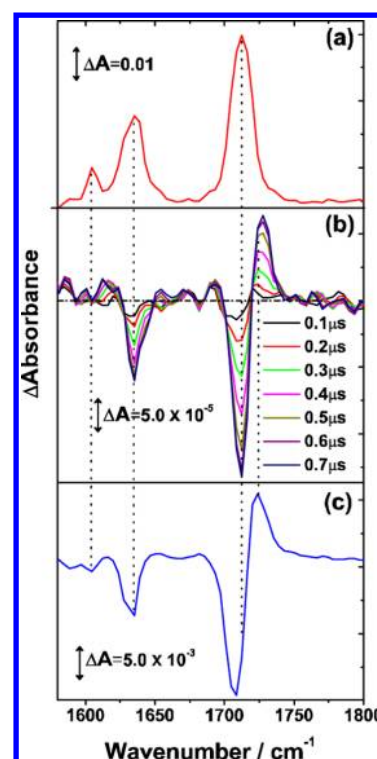
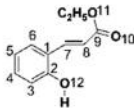
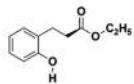
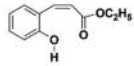
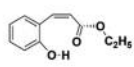
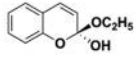
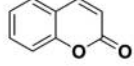


Figure 2. (a) Steady-state IR spectrum of 8 mM HAAEE in acetonitrile, (b) transient IR spectra of 8 mM HAAEE in acetonitrile at selected time delays following 266 nm laser irradiation, and (c) the steady-state difference spectrum of 8 mM HAAEE in acetonitrile after one minute of 266 nm laser irradiation.

bands were observed at 1604 , 1635 , and 1712 cm^{-1} . To aid with spectral assignment, IR frequencies and IR intensities were calculated at the B3LYP/6-311++G(d,p) level for the possible relevant species in the photochemical reaction of HAAEE, both in vacuum and in different solvents with the solvation effect simulated by PCM model (Table 1). The calculated IR frequencies of 1610 , 1637 , and 1693 cm^{-1} for the stable molecule HAAEE in CH_3CN are in good agreement with the experimentally observed frequencies at 1604 , 1635 , and 1712 cm^{-1} , respectively, indicating that the current level of calculation can predict reliable IR frequencies for spectral assignment purpose, particularly for the obtained frequencies under PCM model.

These bands, which arise from double-bond stretches associated with the benzene groups and the carbonyl stretching modes of HAAEE, bleached strongly after one minute of UV exposure as shown in the difference spectra (Figure 2c). Meanwhile, a positive band at 1728 cm^{-1} can be identified, which is the characteristic C=O stretching vibration of the photolyzed coumarin product. To confirm this assignment, the IR spectrum of the authentic sample of coumarin in CH_3CN was recorded (Figure S1, Supporting Information) and found to show a strong C=O absorption at 1733 cm^{-1} and a weak absorption at 1608 cm^{-1} for the C=C stretch of benzene group. The spectral positions of coumarin match those observed in the IR difference spectra (Figure 2c) after UV irradiation, which exhibits a strong positive band at 1728 cm^{-1} and a discernible weak positive band at 1612 cm^{-1} . The small peak shift of 4 or 5 cm^{-1} in the IR difference spectra after UV irradiation is resulted from the partial overlapping of the positive coumarin band with the negative band tail of HAAEE.

Table 1. B3LYP/6-311++G(d,p) Calculated IR Frequencies (cm^{-1}) and IR Intensities for the Possible Relevant Species in the Photochemical Reaction of HAAEE, Both in Vacuum and in Different Solvents with the Solvation Effect Simulated by PCM Model^a

		Gas phase		CH_2Cl_2 solution		CH_3CN solution		H_2O solution		
		mode	cm^{-1}	Intensity km mol^{-1}						
HAAEE(S ₀)		Benzene	1122	88	1121	143	1120	154	1120	157
		Benzene &C7=C8	1617	30	1611	77	1610	90	1610	92
		Benzene	1642	54	1638	198	1637	250	1637	261
		C9=O10	1750	520	1701	1100	1693	1218	1692	1240
HAAEE(T ₁)		C9=O10	1691	178	1665	355	1656	404	1654	414
<i>cis</i> -1		C9-O11 & C2-O12	1205	478	1188	640	1188	732	1188	765
		C7=C8	1682	120	1678	202	1677	213	1677	215
		C9=O10	1739	187	1736	352	1729	402	1727	413
<i>cis</i> -2		C7=C8 & C9-O11	1235	549	1219	1089	1219	1114	1219	1120
		C7=C8	1644	308	1637	453	1635	478	1634	483
		C9=O10	1687	273	1680	448	1675	493	1674	501
Tetrahedral intermediate		C9-O10	1157	322	1139	215	1137	192	1137	188
Coumarin		C9=O10	1804	717	1740	1313	1729	1404	1727	1419

^aThe computed IR intensity in the unit of km mol^{-1} actually denotes the integrated IR absorption coefficient.³¹ Only the vibrational modes with considerable IR intensities are listed here.

The band shapes for the C=O absorption are also similar, with a shoulder at the right-hand side, due to the pronounced anharmonicity of the C=O stretching vibration in coumarin.^{30a} These results, together with the reported vibrational band of coumarin at 1722 cm^{-1} in methylcyclohexane^{30b} and the theoretical prediction of 1729 cm^{-1} in CH_3CN (Table 1), the 1728 cm^{-1} band observed in the IR difference spectra can be confidently assigned to coumarin. Obviously, the band at 1728 cm^{-1} for the photolyzed product coumarin can be distinguished from its caged precursor HAAEE in the IR spectra, which makes it an excellent probe to study the photochemical uncaging reaction dynamics in the time-resolved experiments.

Figure 2b displays the TRIR difference spectra of HAAEE in CH_3CN at typical delay times following 266 nm photolysis. The difference spectra represent the difference between the spectra obtained after photolysis and the spectrum before photolysis. The depletion of reactant gives rise to negative signals, and the formation of transient intermediates or products leads to positive bands. Within the first $0.7 \mu\text{s}$, a prominent positive band at 1728 cm^{-1} is gradually formed, with the negative bands of the HAAEE bleaching at 1635 and 1712 cm^{-1} . After reaching its maximum intensity at $0.7 \mu\text{s}$, the transient positive band at 1728 cm^{-1} does not decay (Figure 3), indicating its identity as a stable photoproduct. This band is a

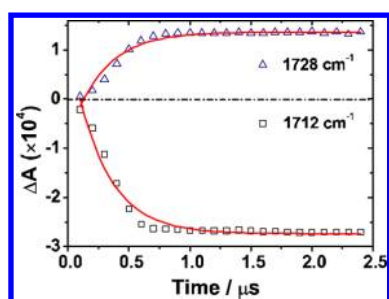


Figure 3. Kinetics traces and the single-exponential fitting curves for the coumarin band at 1728 cm^{-1} and the HAAEE bleaching band at 1712 cm^{-1} .

characteristic vibrational marker band of coumarin, according to its spectral position and band shape. In fact, the excellent agreement between the TRIR spectra and the steady-state IR difference spectrum confirms further that the 1728 cm^{-1} band in the TRIR spectra is ascribed to the stable photoproduct, coumarin, but not transient species such as triplet state of HAAEE or the proposed intermediates of cis-isomer and tetrahedral intermediate. The tetrahedral intermediate simply has no absorption in this spectral range, and the only IR band with considerable intensity for the tetrahedral intermediate is anticipated to be present at 1139 cm^{-1} as shown in Table 1. The expected two pairs of characteristic absorptions for the cis-isomer intermediates, as will be discussed later in the spectra of HAAEE in CH_2Cl_2 , are at the noise level here, indicating negligible amount of cis-isomers present in the spectra of HAAEE photolyzed in CH_3CN .

In addition, all of the transient features observed in the TRIR spectra are shown not to be affected by whether the solution is in air condition, oxygen-saturated, or deaerated with nitrogen. This observation suggests that the photochemical uncaging reaction occurs from a HAAEE singlet excited state, and there is no involvement of the triplet state.

To investigate the rate of release of coumarin due to photolysis of the caged HAAEE, the time evolution of the intensity changes for the 1728 cm^{-1} band was examined (shown in Figure 3 as open triangles). The increase in the intensity of the marker band of coumarin at 1728 cm^{-1} as a function of time is well represented by a single exponential increase, with a rate constant of $3.6 \times 10^6\text{ s}^{-1}$, corresponding to the photorelease rate of coumarin from HAAEE. Concomitantly, the bleaching band of HAAEE at 1712 cm^{-1} follows an almost identical rate of depletion (shown in Figure 3 as open squares), with a rate constant of $3.7 \times 10^6\text{ s}^{-1}$ obtained from the single exponential fitting. Here, the TRIR experiment measures directly the dynamic process of product formation after one laser pulse and thus determines the microscopic uncaging rate noninferentially. It differs from previous steady-state experiments¹¹ also in the aspect that the caged precursor monitored here is the simplest *o*-hydroxycinnamic compound without functional group substitution in the benzene ring and the double bond (Scheme 1).

It shows here in the TRIR spectra that the photochemical uncaging of HAAEE releases coumarin and ethanol rapidly and that the reaction is associated to a singlet excited state. How does the reaction take place? HAAEE represents the typical caged compound containing the *o*-hydroxycinnamic chromophore. It exhibits two absorption bands peaked at 320 and 270 nm (shown in Figure S2, Supporting Information), which can be assigned, respectively, to the excitation to the $S_1(\pi\pi^*)$ and

$S_3(\pi\pi^*)$ states, on the basis of the TD-DFT calculated vertical excitation energies of 95.2 and $106.5\text{ kcal mol}^{-1}$ (shown in Table 2) along with their respective oscillator strengths of 0.27

Table 2. TD-B3LYP/6-311++G(d,p) Calculated Vertical Excitation Energies, Oscillator Strengths (f), and the Dominant Occupied and Virtual Orbitals Contributing to the Three Lowest Energy Singlet Excitations of HAAEE

state	character ^a (% contribution)	energy (eV)	energy (nm)	oscillator strength
S_1	$51 \rightarrow 52$ (62%)	4.14	300	0.27
S_2	$49 \rightarrow 52$ (69%)	4.37	283	0
S_3	$50 \rightarrow 52$ (56%)	4.63	268	0.44

^aOrbital 51 is the highest occupied molecular orbital.

and 0.44. Thus, the excitation wavelength used in this work, 266 nm, corresponds to the strongly dipole allowed transition to $S_3(\pi\pi^*)$ state. According to Kasha's rule,³² the subsequent photochemical or photophysical processes are favorable to take place at the lowest excited state of a given multiplicity no matter which excited state is initially populated. So the highly excited S_3 state is assumed to rapidly internally convert to the lowest lying singlet state $S_1(\pi\pi^*)$, from which the photochemical uncaging of HAAEE is initiated.

The calculated electron density difference plots (Figure 4) suggested that S_1 state corresponds to the $\pi\pi^*$ excitation of the

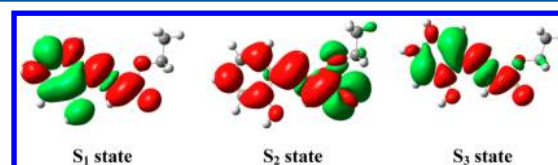


Figure 4. Electron density difference plots for the S_1 , S_2 , and S_3 states of HAAEE calculated at the TD-B3LYP/6-311++G(d,p) level of theory. Isovalue: ± 0.0004 . The green contours represent the depletion of electron density in the ground-state, while the red contours represent the accumulation of electron density in the specific excited state.

conjugated benzene and $\text{C7}=\text{C8}$ moiety such that there is a change in the electron density along the conjugated moiety. The $\pi\pi^*$ excitation of S_1 state is expected to result in a lengthening of the CC double bond and contractions of CC single bonds, a feature that has been proved to allow the trans-cis isomerization to proceed for such kind of ethylenic systems.³³ This corroborates also the observation that there is no triplet state involved in the photochemical reaction of HAAEE.

The trans-cis photoisomerization has been proposed to play key roles in initiating the photochemical uncaging reactions of the *o*-hydroxycinnamic series of compounds.^{9,11} The ground state cis-isomers formed after the trans-cis photoisomerization was proposed to be followed by an intramolecular nucleophilic addition of the *o*-hydroxy group onto the ethyl ester moiety, leading to a tetrahedral intermediate.^{34,35} The intermediate then eliminated ethanol and released the coumarin coproduct, completing the uncaging process. Efforts have been devoted to identify key intermediates with ^1H NMR spectroscopy,^{11,16} and an intermediate containing a double bond with a (*Z*) stereochemistry has been located. However, the identity of this long-lived intermediate captured with ^1H NMR remains unclear because the tetrahedral intermediate and the cis-isomer

intermediates both have identical C7=C8 bond with a (*Z*) stereochemistry, which could not be easily distinguished from each other with ^1H NMR spectroscopy. So we attempted to examine this issue from the TRIR spectra, taking advantage of the IR discerning capability for these two intermediate species. As shown in Table 1 for the predicted vibrational frequencies, the tetrahedral intermediate possesses a vibrational marker band at 1137 or 1139 cm^{-1} (in CH_3CN or CH_2Cl_2) different from those of the *cis*-isomer intermediates, though with a weak IR intensity.

In the polar solvent of CH_3CN , the *cis*-isomers and the tetrahedral intermediate are subject to fast further uncaging reactions, releasing coumarin with a rate of $3.6 \times 10^6 \text{ s}^{-1}$ as has been detected in Figure 3. So the intermediates can not be accumulated with a detectable concentration and can not be easily observed experimentally in this case. In fact, a close inspection of the TRIR spectra for the photolysis in CH_3CN reveals no discernible IR band ascribed to the tetrahedral intermediate in the spectral range around 1137 cm^{-1} , and the expected characteristic absorptions for the *cis*-isomer intermediates are at the noise level. Only the end product coumarin is observed in the TRIR spectra for the photolysis in CH_3CN .

When the photolysis of HAAEE was performed in the apolar solvent CH_2Cl_2 , distinctive results were obtained. In CH_2Cl_2 , the photolysis of HAAEE leads to three ground state bleaching bands at 1603, 1635, and 1712 cm^{-1} together with formation of four positive bands at 1620, 1658, 1689, and 1735 cm^{-1} in the TRIR spectra (Figure 5b). The positive bands are ascribed to stable products but not transient species since the steady-state difference spectra (Figure 5c) also reveal identical bands at

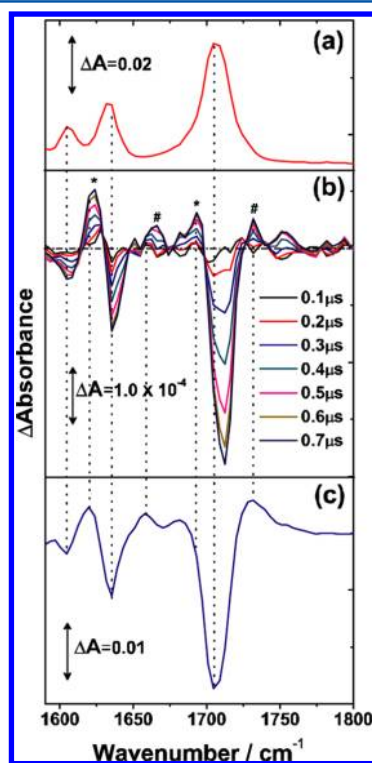


Figure 5. (a) Steady-state IR spectrum of 8 mM HAAEE in CH_2Cl_2 , (b) transient IR spectra of 8 mM HAAEE in CH_2Cl_2 at selected time delays following 266 nm laser irradiation, and (c) steady-state difference spectrum of 8 mM HAAEE in CH_2Cl_2 after one minute of 266 nm laser irradiation.

these positions. According to the spectral position, the four positive bands newly observed in CH_2Cl_2 are ascribed to the *cis*-isomers of HAAEE formed after the *trans*-*cis* photoisomerization. Our B3LYP/6-311++G(d,p) calculations (Table 1) show that the *cis*-isomer of HAAEE has two conformations, *cis*-1 and *cis*-2. The calculated vibrational frequencies of C7=C8 and C9=O10 stretching modes are 1678 and 1736 cm^{-1} for *cis*-1 and 1637 and 1680 cm^{-1} for *cis*-2, in agreement with the four positive bands in Figure 5b,c and thus allow the assignment of the observed bands at 1658 and 1735 cm^{-1} (labeled # in Figure 5) to *cis*-1 and the bands at 1620 and 1689 cm^{-1} (labeled * in Figure 5) to *cis*-2. The identification of the *cis*-isomers in TRIR spectra confirms their existence and validates the key roles of the *trans*-*cis* photoisomerization in initiating the photochemical reaction.

However, the prominent coumarin band at 1728 cm^{-1} observed in CH_3CN is not present in the spectra collected for the photolysis in CH_2Cl_2 , showing that in the less polar solvent CH_2Cl_2 , the *trans*-*cis* photoisomerization is not followed by a further release of the final uncaging products of coumarin and ethanol as in the case of CH_3CN . Obviously, the uncaging reaction subsequent to the *trans*-*cis* photoisomerization is greatly suppressed in less polar solvents of CH_2Cl_2 . Meanwhile, the proposed tetrahedral intermediate is captured in the TRIR spectra for the HAAEE photolysis in CH_2Cl_2 . As can be seen in Figure 6a, a close inspection of the TRIR spectra in the range of 1100–1240 cm^{-1} reveals two positive bands along with a negative band. With the ground state depletion band of HAAEE at 1180 cm^{-1} , two positive bands are present. The one at 1214 cm^{-1} is in excellent agreement with the calculated vibrational frequency for *cis*-2 (1219 cm^{-1}) and thus is assigned to the *cis*-2, which originates from *trans*-*cis* photoisomerization of HAAEE. Same as the other two stronger bands at 1620 and 1689 cm^{-1} , this weak band at 1214 cm^{-1} for the *cis*-2 isomer does not decay after reaching its maximum intensity at 0.7 μs , exhibiting the characteristic as a stable product. Noticeably, the other weak positive band at 1141 cm^{-1} agrees very well with the predicted vibrational frequency of 1139 cm^{-1} for the tetrahedral intermediate. In addition, the band at 1141 cm^{-1} is short-lived. The decay rate of the 1141 cm^{-1} band is obtained to be $3.0 \times 10^5 \text{ s}^{-1}$ from the biexponential fitting for its kinetic trace, as shown in Figure 6b. So the 1141 cm^{-1} band should be ascribed to a transient unstable intermediate, most likely, the tetrahedral intermediate, according to its IR spectral position. This assignment is in line with the previous assumption¹¹ that the tetrahedral intermediate is prone to afford *cis*-isomers by backward reaction and can be further supported by our calculated results that *cis*-1 and *cis*-2 are 9.5 and 14.1 kcal mol^{-1} more stable than the tetrahedral intermediate, respectively (Figure S3, Supporting Information). To the best of our knowledge, this is the first direct spectroscopic evidence revealing the existence of the tetrahedral intermediate, providing support for the previously proposed intramolecular nucleophilic addition mechanism.^{9–13} Here, in the apolar solvent of CH_2Cl_2 , the subsequent reaction of the tetrahedral intermediate releasing coumarin is obviously prohibited, so the tetrahedral intermediate can be detected in the TRIR spectra, unlike the case in the polar solvent of CH_3CN . Because of its instability, the tetrahedral intermediate decays to form the more stable *cis*-isomers by backward reactions, eventually, if not undergoing the forward uncaging of coumarin, as indicated in the calculated energetics diagram (Figure S3, Supporting Information). Therefore, for the

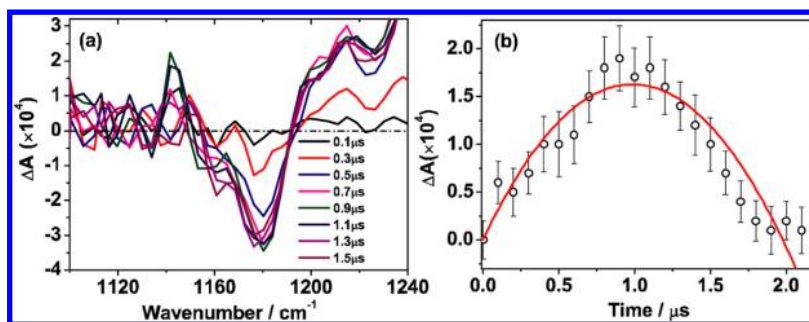


Figure 6. (a) Transient IR spectra of 8 mM HAAEE in CH_2Cl_2 at selected time delays following 266 nm laser irradiation, in the spectral range of 1100–1240 cm^{-1} . The overscaled signal above 1220 cm^{-1} is due to the solvent absorption. (b) Kinetics traces and the biexponential fitting curves for the tetrahedral intermediate band at 1141 cm^{-1} .

photolysis in CH_2Cl_2 when uncaging of coumarin is prohibited, the tetrahedral intermediate are captured as transient unstable intermediate and the cis-isomers are observed as stable photoproducts, whereas no coumarin are detected in the TRIR spectra.

What is the mechanism for the tetrahedral intermediate to release coumarin? It shows in the TRIR experiments that the coumarin yields are greatly affected by the solvent polarity, suppressed greatly in less polar solvents of CH_2Cl_2 (Figure 5) compared to those in the polar solvent of CH_3CN (Figure 2). Such a solvent polarity-dependent behavior indicates that the tetrahedral intermediate most likely undergoes an E1 elimination mechanism, to give rise to the final uncaging product, coumarin. In the E1 elimination, a complex of charge separated ion pair could be produced and serve as an intermediate to produce the final uncaging products (shown in Scheme 2). It is known that the E1 elimination involving charge separation and the intermediate formation of a carbocation could be facilitated in polar solvents, due to the strong effect of solvation on the reaction energetics,³⁶ but in apolar solvent such as CH_2Cl_2 , the E1 elimination is greatly prohibited. The E1 elimination mechanism can explain the observed suppression of coumarin yields in CH_2Cl_2 compared to those in CH_3CN .

To gain further evidence supporting the E1 elimination mechanism of the tetrahedral intermediate, the photolysis of HAAEE was performed in the mixed solvents of $\text{D}_2\text{O}/\text{CH}_3\text{CN}$ with varying water concentration (Figure S4–S7, Supporting Information). The good ionizing and dissociating capability makes water an ideal solvent for the efficient charge separation to occur and thus facilitates the E1 elimination.³⁶ Together with its larger polarity, the addition of water to the solvent is expected to lead to increased reaction rates for the E1 elimination. Indeed, with the addition of 10% D_2O in the mixed $\text{D}_2\text{O}/\text{CH}_3\text{CN}$ solvent (Figure 7a), the amplitude of the coumarin band at 1728 cm^{-1} relative to the HAAEE bleaching band at 1712 cm^{-1} greatly increases compared to that in pure CH_3CN , indicating an increased uncaging product yields at a certain delay time and thus an increased reaction rate. Here, the positive band at 1728 cm^{-1} is partially overlapped with the bleaching band at 1712 cm^{-1} . The real band intensities are therefore obtained by Lorentzian fitting as shown in Figure S8–S9, Supporting Information. The reaction rates can be obtained from the time evolution of the band intensities, by the method of single-exponential fitting as in Figure 3.

The reaction rates of coumarin formation were measured at several water concentrations and are found to increase with the volume ratio of D_2O in the mixed solvents (Figure 7b). It is

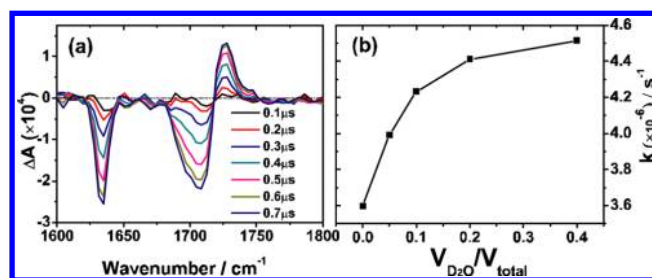


Figure 7. (a) Transient IR spectra of 8 mM HAAEE in D_2O and CH_3CN mixed solvent ($V_{\text{D}_2\text{O}}/V_{\text{total}} = 0.1$) at selected time delays following 266 nm laser irradiation; the corresponding steady-state difference spectrum is shown in Figure S5, Supporting Information; (b) reaction rates of coumarin formation plotted as a function of water concentration.

interesting to note that, for solvents with water content larger than 20%, the increase of the reaction rates becomes much more modest upon further addition of water to the solvent. The measured reaction rates follow a curved dependence on water concentration (Figure 7b). This indicates the predominant role of the solvent water molecules in the inner solvation shell to promote the reaction at large water concentrations.

4. CONCLUSIONS

In this work, we have performed time-resolved infrared detection of the photochemical uncaging reaction for the *o*-hydroxycinnamic phototrigger compound HAAEE. By taking advantage of the specific vibrational marker bands and the IR discerning capability, we have identified and distinguished two key intermediate species, the cis-isomers of HAAEE and the tetrahedral intermediate, in the transient infrared spectra, thus providing clear spectral evidence to support the previously proposed intramolecular nucleophilic addition mechanism following the trans–cis photoisomerization. Moreover, by detecting the photolysis in different solvents, we observed that the product yield of coumarin upon uncaging is greatly affected by the solvent polarity, suppressed in CH_2Cl_2 but enhanced in $\text{D}_2\text{O}/\text{CH}_3\text{CN}$ with the increasing volume ratio of D_2O . The highly solvent-dependent behavior indicates an E1 elimination mechanism of the tetrahedral intermediate to give rise to the final uncaging product coumarin.

Additionally, we show here that photoexcitation of HAAEE gives rise to good yields of ethanol with coumarin coproduct in polar solvents of CH_3CN or $\text{D}_2\text{O}/\text{CH}_3\text{CN}$ rapidly (rate measured to be $3.6 \times 10^6 \text{ s}^{-1}$ by the direct, noninferential TRIR method). It is thus anticipated that the *o*-hydroxycinnamic caged compounds such as HAAEE hold promise for use in

producing fast and robust alcohol jumps with fluorescence reporting. The dependence of the product yields and reaction rates on the solvent polarity would implicate that the quantity of uncaged alcohols could be modulated by the polarity of the local environment of biological cells or tissues, which should also be noteworthy in biological applications.

■ ASSOCIATED CONTENT

■ Supporting Information

Additional computational and experimental results. This material is available free of charge via the Internet at <http://pubs.acs.org>.

■ AUTHOR INFORMATION

■ Corresponding Author

*(H.S.) E-mail: hongmei@iccas.ac.cn.

■ Notes

The authors declare no competing financial interest.

■ ACKNOWLEDGMENTS

This work is financially supported by the National Natural Science Foundation of China (Grant No. 21073201) and the National Basic Research Program of China (No. 2013CB834602).

■ REFERENCES

- (1) Ellis-Davies, G. C. R. Caged Compounds: Photorelease Technology for Control of Cellular Chemistry and Physiology. *Nat. Methods* **2007**, *4*, 619–628.
- (2) Klan, P.; Pelliccioli, A. P.; Pospisil, T.; Wirz, J. 2,5-Dimethylphenacyl Esters: A Photoremovable Protecting Group for Phosphates and Sulfonic Acids. *Photochem. Photobiol. Sci.* **2002**, *1*, 920–923.
- (3) Mayer, G.; Heckel, A. Biologically Active Molecules with a "Light Switch". *Angew. Chem., Int. Ed.* **2006**, *45*, 4900–4921.
- (4) Sankaranarayanan, J.; Muthukrishnan, S.; Gudmundsdottir, A. D. Photoremovable Protecting Groups Based on Photoenolization. In *Advances in Physical Organic Chemistry*; Academic Press Ltd–Elsevier Science Ltd: London, U.K., 2009; Vol. 43, pp 39–77.
- (5) Ackmann, A. J.; Frechet, J. M. J. The Generation of Hydroxide and Methoxide Ions by Photo-Irradiation: Use of Aromatization to Stabilize Ionic Photo-Products from Acridine Derivatives. *Chem. Commun.* **1996**, 605–606.
- (6) Suzuki, A. Z.; Watanabe, T.; Kawamoto, M.; Nishiyama, K.; Yamashita, H.; Ishii, M.; Iwamura, M.; Furuta, T. Coumarin-4-Ylmethoxycarbonyls as Phototriggers for Alcohols and Phenols. *Org. Lett.* **2003**, *5*, 4867–4870.
- (7) Ma, C. S.; Kwok, W. M.; Chan, W. S.; Du, Y.; Kan, J. T. W.; Toy, P. H.; Phillips, D. L. Ultrafast Time-Resolved Transient Absorption and Resonance Raman Spectroscopy Study of the Photodeprotection and Rearrangement Reactions of *p*-Hydroxyphenacyl Caged Phosphates. *J. Am. Chem. Soc.* **2006**, *128*, 2558–2570.
- (8) Cheng, Q.; Steinmetz, M. G.; Jayaraman, V. Photolysis of Gamma-(alpha-carboxy-2-nitrobenzyl)-L-glutamic Acid Investigated in the Microsecond Time Scale by Time-Resolved FTIR. *J. Am. Chem. Soc.* **2002**, *124*, 7676–7677.
- (9) Turner, A. D.; Pizzo, S. V.; Rozakis, G.; Porter, N. A. Photoreactivation of Irreversibly Inhibited Serine Proteinases. *J. Am. Chem. Soc.* **1988**, *110*, 244–250.
- (10) Li, H.; Yang, J. H.; Porter, N. A. Preparation and Photochemistry of *o*-Aminocinnamates. *J. Photochem. Photobiol., A* **2005**, *169*, 289–297.
- (11) Gagey, N.; Neveu, P.; Benbrahim, C.; Goetz, B.; Aujard, I.; Baudin, J.-B.; Jullien, L. Two-Photon Uncaging with Fluorescence Reporting: Evaluation of the *o*-Hydroxycinnamic Platform. *J. Am. Chem. Soc.* **2007**, *129*, 9986–9998.
- (12) Gagey, N.; Neveu, P.; Jullien, L. Two-Photon Uncaging with the Efficient 3,5-Dibromo-2,4-Dihydroxycinnamic Caging Group. *Angew. Chem., Int. Ed.* **2007**, *46*, 2467–2469.
- (13) Gagey, N.; Emond, M.; Neveu, P.; Benbrahim, C.; Goetz, B.; Aujard, I.; Baudin, J.-B.; Jullien, L. Alcohol Uncaging with Fluorescence Reporting: Evaluation of *o*-Acetoxyphenyl Methyloxazolone Precursors. *Org. Lett.* **2008**, *10*, 2341–2344.
- (14) Goppert, M. The Probability of Two Photons Cooperating in One Elementary Act. *Naturwissenschaften* **1929**, *17*, 932–932.
- (15) Goppert-Mayer, M. Elementary File with Two Quantum Fissures. *Ann. Phys.* **1931**, *9*, 273–294.
- (16) Duan, X. Y.; Zhai, B. C.; Song, Q. H. Water-Soluble *o*-Hydroxycinnamate as an Efficient Photoremovable Protecting Group of Alcohols with Fluorescence Reporting. *Photochem. Photobiol. Sci.* **2012**, *11*, 593–598.
- (17) Lee, Y. P. State-Resolved Dynamics of Photofragmentation. *Annu. Rev. Phys. Chem.* **2003**, *54*, 215–244.
- (18) Conrad, P. G.; Givens, R. S.; Hellrung, B.; Rajesh, C. S.; Ramseier, M.; Wirz, J. *p*-Hydroxyphenacyl Phototriggers: The Reactive Excited State of Phosphate Photorelease. *J. Am. Chem. Soc.* **2000**, *122*, 9346–9347.
- (19) Hess, G. P.; Grewer, C. Development and Application of Caged Ligands for Neurotransmitter Receptors in Transient Kinetic and Neuronal Circuit Mapping Studies. *Methods Enzymol.* **1998**, *291*, 443–473.
- (20) Gee, K. R.; Carpenter, B. K.; Hess, G. P. Synthesis, Photochemistry, and Biological Characterization of Photolabile Protecting Groups for Carboxylic Acids and Neurotransmitters. *Methods Enzymol.* **1998**, *291*, 30–50.
- (21) Uhmann, W.; Becker, A.; Taran, C.; Siebert, F. Time-Resolved FT-IR Absorption-Spectroscopy Using a Step-Scan Interferometer. *Appl. Spectrosc.* **1991**, *45*, 390–397.
- (22) Drapcho, D. L.; Curbelo, R.; Jiang, E. Y.; Crocombe, R. A.; McCarthy, W. J. Digital Signal Processing for Step-Scan Fourier Transform Infrared Photoacoustic Spectroscopy. *Appl. Spectrosc.* **1997**, *51*, 453–460.
- (23) Wu, W. Q.; Liu, K. H.; Yang, C. F.; Zhao, H. M.; Wang, H.; Yu, Y. Q.; Su, H. M. Reaction Mechanisms of a Photo-Induced [1,3] Sigmatropic Rearrangement Via a Nonadiabatic Pathway. *J. Phys. Chem. A* **2009**, *113*, 13892–13900.
- (24) Becke, A. D. Density-Functional Thermochemistry 0.3. The Role of Exact Exchange. *J. Chem. Phys.* **1993**, *98*, 5648–5652.
- (25) Lee, C. T.; Yang, W. T.; Parr, R. G. Development of the Colle–Salvetti Correlation-Energy Formula into a Functional of the Electron-Density. *Phys. Rev. B* **1988**, *37*, 785–789.
- (26) Gonzalez, C.; Schlegel, H. B. Reaction-Path Following in Mass-Weighted Internal Coordinates. *J. Phys. Chem.* **1990**, *94*, 5523–5527.
- (27) Tomasi, J.; Persico, M. Molecular-Interactions in Solution: An Overview of Methods Based on Continuous Distributions of the Solvent. *Chem. Rev.* **1994**, *94*, 2027–2094.
- (28) Cramer, C. J.; Truhlar, D. G. Implicit Solvation Models: Equilibria, Structure, Spectra, and Dynamics. *Chem. Rev.* **1999**, *99*, 2161–2200.
- (29) Frisch, M. J.; Trucks, G. W.; Schlegel, H. B.; Scuseria, G. E.; Robb, M. A.; Cheeseman, J. R.; Scalmani, G.; Barone, V.; Mennucci, B.; Petersson, G. A.; et al. *Gaussian 09*, revision A.02; Gaussian, Inc.: Wallingford, CT, 2009.
- (30) (a) Kus, N.; Breda, S.; Reva, I.; Tasal, E.; Ogretir, C.; Fausto, R. FTIR Spectroscopic and Theoretical Study of the Photochemistry of Matrix-Isolated Coumarin. *Photochem. Photobiol.* **2007**, *83*, 1541–1542. (b) Wolff, T.; Goerner, H. Photocleavage of Dimers of Coumarin and 6-Alkylcoumarins. *J. Photochem. Photobiol., A* **2010**, *209*, 219–223.
- (31) Hess, B. A.; Schaad, L. J.; Carsky, P.; Zahradnik, R. Ab Initio Calculations of Vibrational-Spectra and Their Use in the Identification of Unusual Molecules. *Chem. Rev.* **1986**, *86*, 709–730.
- (32) Kasha, M. Characterization of Electronic Transitions in Complex Molecules. *Discuss. Faraday Soc.* **1950**, 14–19.

(33) Gonzalez-Luque, R.; Garavelli, M.; Bernardi, F.; Merchan, M.; Robb, M. A.; Olivucci, M. Computational Evidence in Favor of a Two-State, Two-Mode Model of the Retinal Chromophore Photoisomerization. *Proc. Natl. Acad. Sci. U.S.A.* **2000**, *97*, 9379–9384.

(34) Hershfie, R.; Schmir, G. L. Lactonization of Coumarinic Acids: Kinetic Evidence for Three Species of Tetrahedral Intermediate. *J. Am. Chem. Soc.* **1973**, *95*, 8032–8040.

(35) Hershfie, R.; Schmir, G. L. Lactonization of Ring-Substituted Coumarinic Acids: Structural Effects on Partitioning of Tetrahedral Intermediates in Esterification. *J. Am. Chem. Soc.* **1973**, *95*, 7359–7369.

(36) Reichardt, C. *Solvent and Solvent Effect in Organic Chemistry*; VCH Verlagsgesellschaft mbH: Weinheim, Germany, 1988.